Ragab A. Sayed*[1], Sabry Allam[1], Sheeraz Iqbal[2], Md Shafiullah[2], Muhammad Aurangzeb[3], Hossam Youssef Hegazy[4], and Samia Abdel Fattah[4]

J. Electrical Systems 21-2 (2025): 208-235

Regular paper

Optimal Design and Simulation of an Artificial Neural Network Control System to Optimize Energy Management in a Hybrid Electric Vehicle

This paper presents an advanced control system that utilizes artificial neural networks (ANN) to optimize energy management in hybrid electric vehicles (HEVs) that combine fuel cells, photovoltaic panels, and batteries. The primary objective is to enhance the utilization of these energy sources to improve efficiency, reduce emissions, and extend the operating range of the vehicle. The study involves developing a comprehensive model of the vehicle s energy flow and training the ANN for informed real-time decision-making. The performance of the system is evaluated through simulations and experimental validations. The research adopts a model-based approach to assess the feasibility of a photovoltaic-fuel cell-battery hybrid electric vehicle (PVFCHEV), contributing to two key advances: building a detailed PVFCHEV system model in MATLAB/Simulink and introducing an ANN-based energy management strategy (EMS) to optimize solar energy utilization. Simulation results under various driving conditions, including different levels of solar radiation and battery states, demonstrate the effectiveness of the system. The proposed EMS achieves superior fuel economy compared to traditional PID control methods, highlighting the potential of renewable energy sources to address global warming challenges. The development of this ANN-based control system for electric vehicles showcases significant potential for optimizing energy management and enhancing vehicle efficiency and sustainability. Future research should focus on further refinement of the ANN architecture and exploring its scalability for various vehicle types and driving conditions.

Keywords: Artificial neural networks (ANN), Hybrid Electric Vehicles (HEVs), Fuel Cells (FCs), Energy Management Systems (EMS), and Photovoltaic panels (PV).

1 Introduction

The exponential growth of global energy demand has led to a significant increase in greenhouse gas emissions, requiring the industrial and academic sectors around the world to seek alternative energy sources [1]. The ecological and economic need to improve the transportation sector has resulted in the rise of electric vehicles based on renewable energy, which are expected to dominate the automobile market in the coming years [2]. Greenhouse gas emissions pose a global challenge with serious implications for the environment and public health [3]. Electric vehicles offer a promising solution, as they produce significantly lower emissions compared to traditional gasoline vehicles [4].

* Corresponding author: Ragab A. Sayed, Automotive Technology Department, Faculty of Technology and Education, Helwan University, Cairo, Egypt., E-mail: eng.ragab9686@gmail.com

1 Automotive Technology Department, Faculty of Technology and Education, Helwan University, Cairo, Egypt.

2 Interdisciplinary Research Center for Sustainable Energy Systems, Research and Innovation, King Fahd University of Petroleum & Minerals, Dhahran 31261, Saudi Arabia.

3 School of Electrical Engineering, Southeast University, Nanjing, China.

4 Electrical Technology Department, Faculty of Technology and Education, Helwan University, Cairo, Egypt.

This transition would reduce reliance on fossil fuels, decrease greenhouse gas emissions, and provide economic benefits through job creation and sustainable energy sources [5]. Overall, this shift is essential for mitigating climate change and advancing sustainable development [6]. The recent integration of solar energy into electric vehicles marks a significant step away from fossil fuel dependency [7]. This approach is particularly advantageous in the equatorial and Mediterranean regions, such as Algeria, where solar radiation is abundant [8]. Energy can be harvested using photovoltaic panels installed on the vehicle's roof or through a photovoltaic coating that covers the entire car [9].

The collected energy can power auxiliary systems such as lights and air conditioning while also reducing the depletion of the vehicle's battery [10]. Several car manufacturers, from established brands like Tesla, Audi, Mercedes-Benz, BMW, Jaguar, and Honda to emerging startups such as Stella Lux, Hanergy, Fisker, Sono Motors, and Lightyear, have embraced the concept of electric vehicles with integrated photovoltaic panels [11].

Over the past few decades, several scholars have conducted in-depth studies on power management solutions [12]. Academics have categorized and described various approaches used to optimize gas emissions and fuel consumption in hybrid electric vehicles [13]. These techniques can be broadly divided into two categories: online and offline power management strategies [14]. Offline strategies require prior knowledge of global information to determine the best solution, which makes real-time implementation challenging [15]. Power management solutions offer both advantages and disadvantages [16]. They can enhance energy efficiency, reduce costs, increase reliability, and facilitate the integration of renewable energy [17]. However, drawbacks include high implementation costs, the need for specialized expertise, and the potential for system failures.

ANNs typically divide a global optimization problem into smaller subproblems and then explore various control inputs to identify the minimal cost final solution [18]. However, ANNs cannot be applied in real-time on a vehicle due to their need for prior knowledge of the complete drive cycle and their high computational demands. Consequently, the findings from ANN simulations will serve as an ideal reference control method for this research [19]. This study has developed an intelligent power management system for hybrid electric vehicles that optimizes energy flow among the battery, fuel cells, and photovoltaic panels. The system predicts energy demand and adjusts power flow in real time, enhancing energy efficiency and performance while reducing reliance on non-renewable energy sources. This advancement not only lowers the vehicle's carbon footprint but also contributes to a more sustainable transportation system.

This article presents two significant original contributions aligned with the stated objectives. First, it introduces a comprehensive Simulink physical model of a 6 kW lightweight PVFCHEV, developed using verified Simscape components. This model encompasses the entire electrical system, control system, and vehicle dynamics, allowing for credible and precise validation of the PVFCHEV structure. Second, it establishes an Energy Management System for the PVFCHEV based on an ANN strategy. Unlike a standard fuel cell electric vehicle (FC EV), this model includes a signal port for solar power and features reasoning rules specifically designed to optimize solar energy usage. Finally, both the model and the EMS are validated through simulations that include functional and driving cycle tests, addressing rapidly changing driving power demands, variations in solar power, and different battery statuses.

2 SYSTEM MANAGEMENT STUDIED BY ARTIFICIAL NEURAL NETWORKS

2.1 Designing and programming ANN models

Artificial Neural Network (ANN) is a novel computing technology in the field of computer science studies and one of the studies of Artificial Intelligence. Pattern recognition, data

analysis, and control are the most common applications for neural networks. Knowledge of the nervous system, particularly the human brain and its densely coupled neurons, inspired the central concept. Because of their high nonlinearity, massive volumes of data-parallel processing, and high robustness, artificial neural networks (ANN) are one of the methods that are suited for dealing with the internal relations of a complicated model [20].

To experimentally investigate artificial neural network-based power management for hybrid electric vehicles, a prototype system must be designed and implemented, followed by testing under different conditions. Suitable components must be selected based on their compatibility and suitability for the electric vehicle application, such as PV panels, batteries, fuel cells, DC-DC converter, DC-AC inverter, and AC motor. The artificial neural network-based power management system would monitor the motor's power demand and optimize the power flow from the PV panel, battery, and fuel cells to the electric motor. Experiments should evaluate the system's performance under various conditions, and data collected during testing should be analyzed to assess the accuracy of the neural network's predictions and the effectiveness of the system in optimizing power flow.

2.2 Training base

2.2.1 Adapting measurements for neural network inputs

To simplify the neural network and process all potential values, we can utilize the numbering of variation intervals for the measured quantities as neural network inputs. The adaptation of measurements for neural network inputs is illustrated in Table 1.

Table 1. Adapting measurements for neural network inputs.

Size Measured	Variation Interval	Interval Numbering (Specification of neural network inputs)
Battery SOC	SOC ≤ 33%	1
	33% < SOC ≤ 66%	2
	SOC > 66%	3
PV power	PV ≤ 33%	1
	33% < PV ≤ 66%	2
	PV > 66%	3
Power demand	Power demand = 20 (Very Small)	1
	Power demand = 40 (Small)	2
	Power demand = 60 (Medium)	3
	Power demand = 80 (Large)	4
	Power demand = 100 (Very Large)	5

Depending on the measurement of these chosen parameters and depending on the digitized intervals, the final structure of the neural network will be presented in the following section.

2.2.2 The final structure used

Figure 1 illustrates the ultimate architecture utilized as the training base, which is composed of three main components: (1) an input layer for independent variables, (2) one or more hidden layers, and (3) an output layer for the dependent variable.

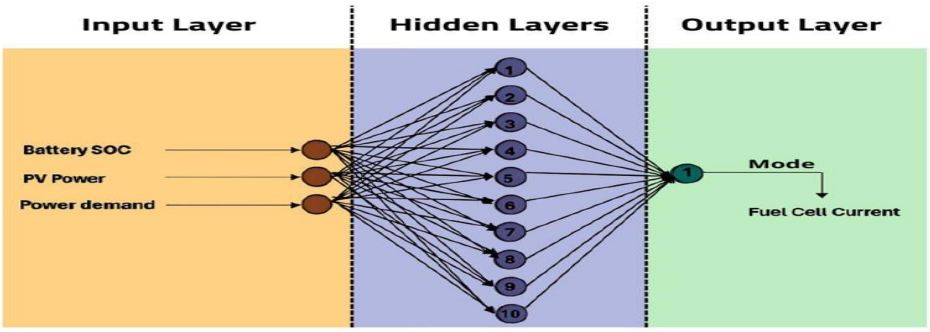

Figure 1. Power management-based neural network model architecture.

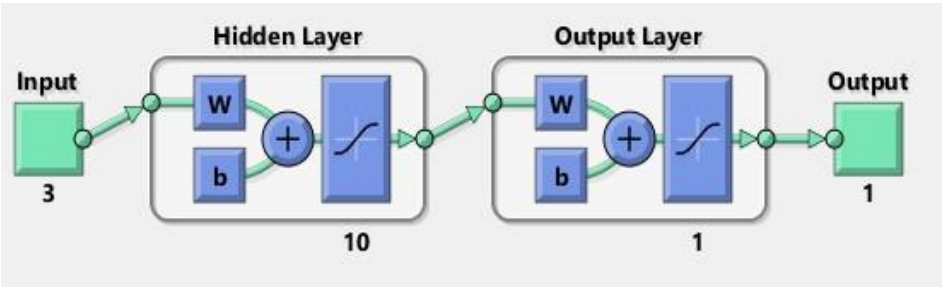

Figure 2. Power management-based neural network model architecture on MATLAB Simulink.

Designing a power management system using a neural network model on MATLAB Simulink involves several steps (Figure 2). In this case, we will provide a high-level overview of the process involved in developing a power management system using a neural network model in MATLAB Simulink.

- Define the problem statement: The first step in developing a power management system using a neural network model is to define the problem statement. This involves identifying the key requirements of the power management system, such as the input and output parameters, constraints, and performance metrics.
- Data collection and preprocessing: The next step is to collect the data that will be used to train the neural network model. This may include data on the energy consumption of different devices, the availability of renewable energy sources, and other relevant parameters. The data may need to be preprocessed to remove noise and outliers, normalize the data, and split it into training and testing sets.
- Neural network model selection and design: Once the data has been collected and preprocessed, the next step is to select an appropriate neural network model for the power management system. This may involve choosing between different types of neural networks, such as feedforward, recurrent, or convolutional neural networks. The architecture of the neural network model must be designed, taking into account the problem statement and the data available.
- Training the neural network model: The neural network model is then trained using a train using a feedforward neural network. During the training process of a neural

network, the weights and biases are modified to minimize the difference between the predicted and actual output values.

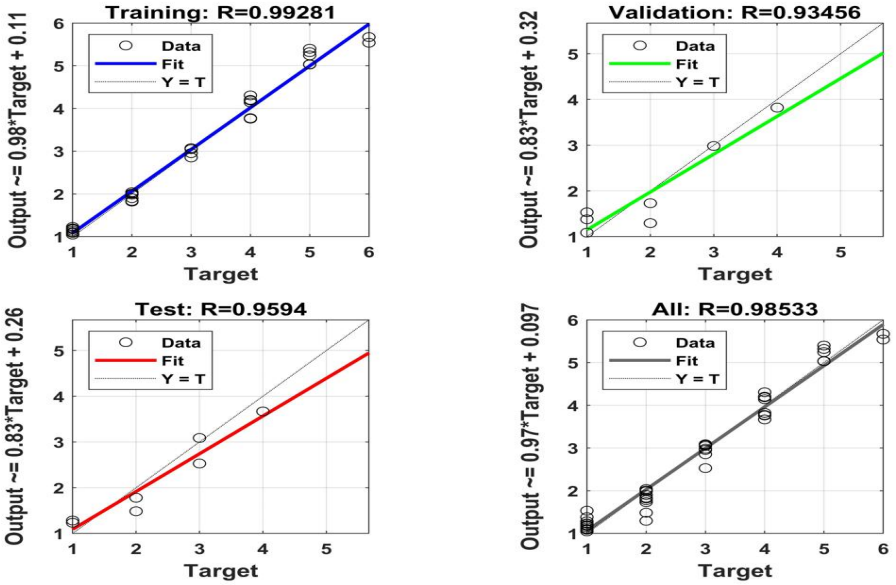

Figure 3. The obtained target-based training process.

- Testing and validation: After the neural network model has been trained, it is tested using the testing set of data to evaluate its performance (Figure 3). To assess the effectiveness of the neural network model, metrics like mean squared error, mean absolute error, and accuracy are utilized.
- Implementation in MATLAB Simulink: Once the neural network model has been trained and validated, it can be implemented in MATLAB Simulink as a power management system. The input parameters of the power management system are fed into the neural network model, which outputs the optimal power allocation to different devices based on the input parameters and the constraints.
- Performance evaluation: The performance of the power management system can be evaluated based on its ability to meet the performance metrics defined in the problem statement. The power management system may need to be refined and retrained if it does not meet the desired performance metrics.

The driving modes of operation used in the power management algorithm are listed in Table 2; those modes are already mentioned below.

Table 2. Neural network outputs.

Mode	Output Value (Fuel Current)
Mode 0	**ZE (Zero)**
Mode 1	**VS (Very Small)**
Mode 2	**S (Small)**
Mode 3	**M (Medium)**
Mode 4	**L (Large)**
Mode 5	**VL (Very Large)**

In this study, the following operation modes of the hybrid electric vehicle are proposed:

- Shutdown mode (mode 0): This mode is activated when the hybrid electric vehicle is completely turned off. The electrical system is deactivated, and all vehicle functions are out of service.
- Starting mode (mode 1): This mode is activated when the driver turns on the hybrid electric vehicle.
- Acceleration mode (mode 2): This mode is activated when the driver presses the accelerator pedal, and the electric motor increases the vehicle's speed.
- Operation at nominal speed (mode 3): This mode is activated when the vehicle is moving at a steady speed, and the electric motor is maintaining that speed.
- Constant speed or cruise mode (mode 4): This mode is activated when the driver sets the vehicle to maintain a constant speed, often used during highway driving.
- Deceleration or braking mode (mode 5): This mode is activated when the driver applies the brakes or reduces the accelerator pedal, and the electric motor slows down the vehicle. In some hybrid electric vehicles, this mode can also regenerate energy back into the battery.

2.2.3 Data Preparation

The dataset used for training the ANN was created using an Excel sheet and uploaded into MATLAB. The data consists of:

Inputs (3x45):

- Battery SOC levels: Low (1), Medium (2), High (3)
- PV power levels: Low (1), Medium (2), High (3)
- Power demand levels: Very Small (20), Small (40), Medium (80), Large (100), Very Large

Output (1x45):

- Fuel cell current: Zero (ZE), Very Small (VS), Small (S), Medium (M), Large (L), Very Large (VL)

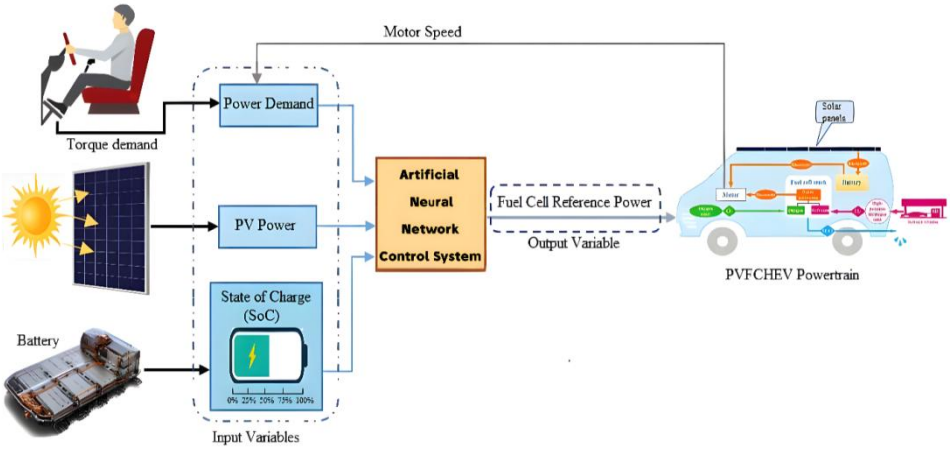

Figure 4. The diagram illustrates the energy management strategy based on ANN. The main components include photovoltaic systems (PV), photovoltaic-fuel cell-battery hybrid electric vehicles (PVFCHEV), and state of charge (SOC).

2.2.4 Training table

Table 3 summarizes the training table for the learning method based on neural networks for the energy management of a hybrid electric vehicle, which will be implemented under MATLAB/Simulink.

Table 3. Training table.

Operating conditions	Inputs			Output	Operating conditions	Inputs			Output
	Battery SOC	PV power	Power demand	Fuel cell current		Battery SOC	PV power	Power demand	Fuel cell current
S1	1	1	20	2	S24	3	1	60	2
S2	1	2	20	2	S25	3	2	60	1
S3	2	1	20	1	S26	2	3	60	2
S4	2	2	20	1	S27	3	3	60	1
S5	1	3	20	2	S28	1	1	80	5
S6	3	1	20	1	S29	1	2	80	5
S7	3	2	20	1	S30	2	1	80	4
S8	2	3	20	1	S31	2	2	80	4
S9	3	3	20	1	S32	1	3	80	4
S10	1	1	40	4	S33	3	1	80	2
S11	1	2	40	3	S34	3	2	80	2
S12	2	1	40	2	S35	2	3	80	3
S13	2	2	40	2	S36	3	3	80	1
S14	1	3	40	3	S37	1	1	100	6
S15	3	1	40	1	S38	1	2	100	6
S16	3	2	40	1	S39	2	1	100	5
S17	2	3	40	1	S40	2	2	100	4
S18	3	3	40	1	S41	1	3	100	5
S19	1	1	60	5	S42	3	1	100	3
S20	1	2	60	4	S43	3	2	100	3
S21	2	1	60	3	S44	2	3	100	4
S22	2	2	60	3	S45	3	3	100	2
S23	1	3	60	4					

3 DESCRIPTION OF THE STUDIED SYSTEM

This paper outlines the development of a PVFCHEV system model in MATLAB/Simulink, utilizing the Sim Power Systems package. It establishes a comprehensive physical modeling environment where various predefined components are interconnected, facilitating the modeling, simulation, and analysis of electromechanical systems. This approach enables an accurate representation of the system's architecture through block diagrams, which allows for the automatic generation of system-level equations. The PVFCHEV system model consists of three main subsystems: the electrical system, the energy management system, and the vehicle dynamics system, as illustrated in Figures 5 and 6.

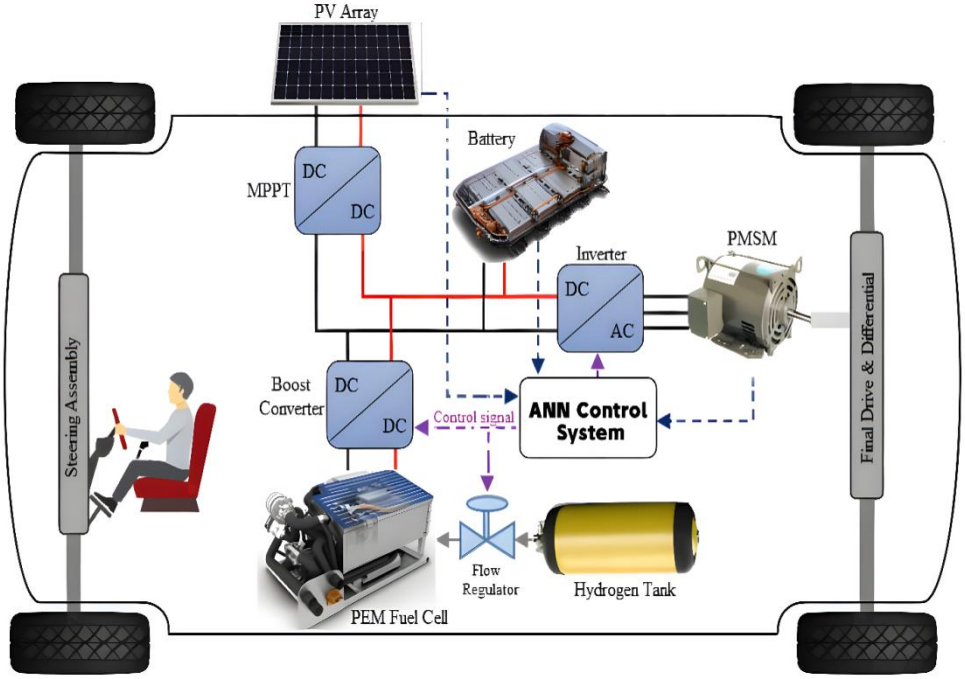

Figure 5. The structure of a PV-FC-battery HEV. HEV refers to hybrid electric vehicles; MPPT denotes maximum power point tracking; PEM signifies proton exchange membrane; PMSM represents permanent magnet synchronous machine; and PV-FC indicates photovoltaic-fuel cell.

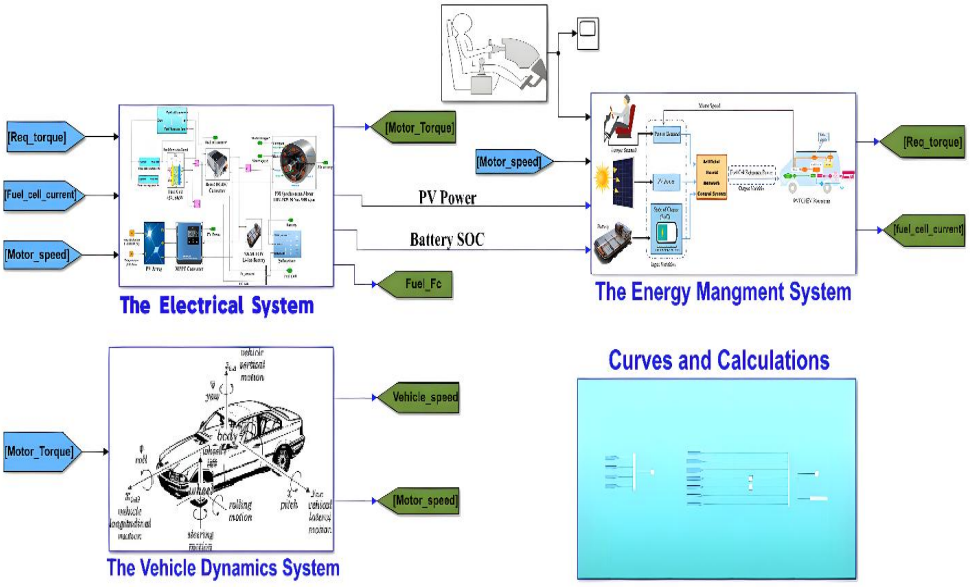

Figure 6. A diagram illustrating the three systems of a photovoltaic-fuel cell-battery hybrid electric vehicle (PV-FC-battery HEV).

Figures 5 and 6 depict the structure of the PVFCHEV system, which comprises a rooftop photovoltaic (PV) array, a proton exchange membrane fuel cell (PEMFC) stack, a high-pressure hydrogen tank, a lithium-ion battery as a secondary power source, a supervisory controller, and an electric motor with an inverter. The PV array connects to a maximum power point tracking (MPPT) converter to optimize power output. When the vehicle is stationary or decelerating, excess solar energy is stored in the battery. The PEMFC stack acts as the primary power source, supplying energy to the electric motor, while any surplus electricity generated by the fuel cell recharges the battery. A flow rate regulator controls the hydrogen flow from the tank, reducing pressure and adjusting the flow rate to modulate the fuel cell's power output.

The lithium-ion battery is chosen for its high-power density and rapid response, allowing it to meet transient power demands and capture excess energy during regenerative braking [21]. A permanent magnet synchronous machine (PMSM) is utilized as the electric motor [22] due to its efficiency and reliability. The supervisory controller continuously monitors the system's status, including the power output of the PV array, the state of charge (SOC) of the battery, and power demand, to regulate both the fuel cell's power output and the motor's torque.

3.1 Energy management system

The energy management system produces reference signals for both the motor drive and the DC/DC converter of the fuel cell, facilitating efficient power distribution among different electrical sources.

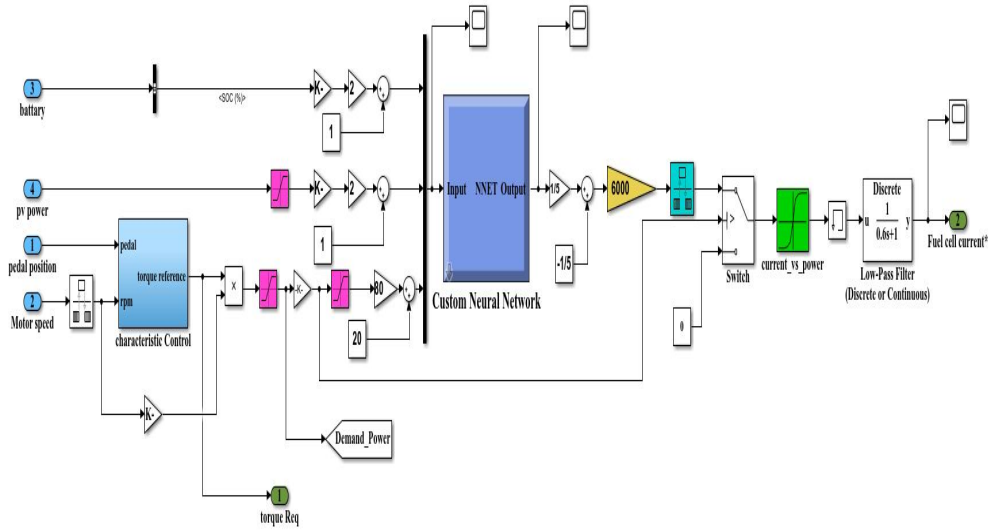

Figure 7. The block diagram of the energy management system. SOC, state-of-charge.

Figure 7 illustrates the system's block diagram, which processes four input signals: battery state of charge (SOC), photovoltaic (PV) power, pedal position, and motor speed. The pedal position signal is generated by the Longitudinal Driver block in Simulink, utilizing a PID controller [23] to produce normalized pedal signals that correspond to the speed profile

of a specified driving cycle. Power demand is determined by multiplying the required motor torque by the motor speed.

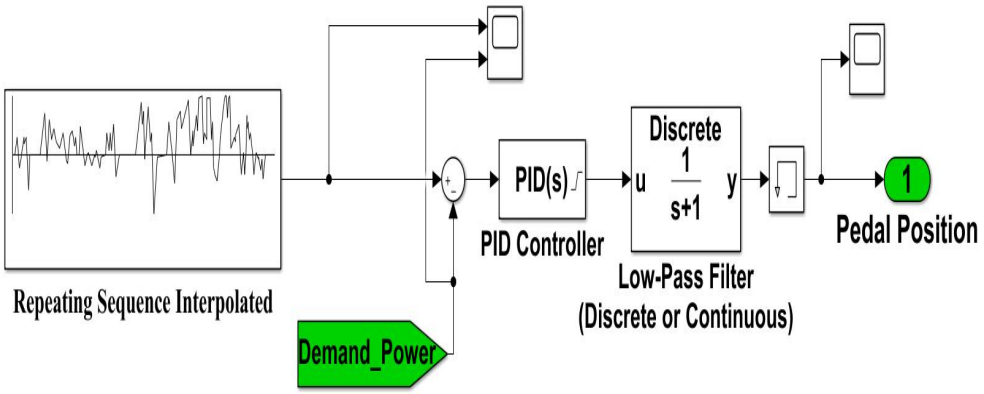

Figure 8. The block diagram of the pedal position signal generation.

The input parameters for PV power (P_{PV}) and driving power demand (P_{demand}) are scaled to a range of 0 to 1 using the following equations [24]:

$$\boldsymbol{\theta(P_{PV})} = \frac{\boldsymbol{P_{PV}}}{\boldsymbol{P_{PV}^{max}}} \quad \textbf{(1)}$$

$$\boldsymbol{\theta(P_{demand})} = \frac{\boldsymbol{P_{demand}}}{\boldsymbol{P_{demand}^{max}}} \quad \textbf{(2)}$$

Of the motor, respectively. The ANN controller employs the control strategy outlined in Section 2.2.3. By inputting the Where P_{PV}^{max} and $P_{\text{demand}}^{\max}$ Representing the maximum power of the PV array and the peak power parameters of battery state of charge (SOC), solar power, and motor power demand, the controller generates the parameter $\theta(P_{FC})$, which is then used as the reference power for the fuel cell (FC) as follows [25]:

$$\boldsymbol{P_{FC}} = \boldsymbol{\alpha\theta(P_{FC})} \quad \textbf{(3)}$$

Where α is the proportional gain and P_{FC} is the reference power of the fuel cell (FC). The reference power is converted into the reference current using the polarization curve of the FC. The lifespan of the FC can be significantly reduced if its operating conditions undergo frequent and drastic changes. To mitigate the degradation of the FC, a raté limiter restricts the rate of change of FC power to within 0.5 kW/s. It is important to note that, in this study, the power range for operating the FC system is between 0.6 and 6 kW, with the motor's peak power at 5 kW and the maximum power of the photovoltaic (PV) array at 0.5 kW.

3.2 Electrical system

The electrical system consists of four main components: à photovoltaic (PV) array with a maximum power point tracking (MPPT) converter, a lithium-ion (Li-ion) battery, a proton exchange membrane fuel cell (PEMFC) with a boost converter, and a motor. The MPPT converter boosts the low voltage produced by the PV array to the higher voltage required for the direct current (DC) bus while optimizing the solar panels' power output [26]. The boost converter associated with the PEMFC regulates the fuel cell's output power through current management, employing a proportional-integral (PI) control technique [27]. Additionally, the battery connected to the DC bus provides extra power for system startup and helps restore the state of charge (SOC) through regenerative braking and surplus energy from the fuel cell. Figure 9 illustrates the block diagram of the electrical system.

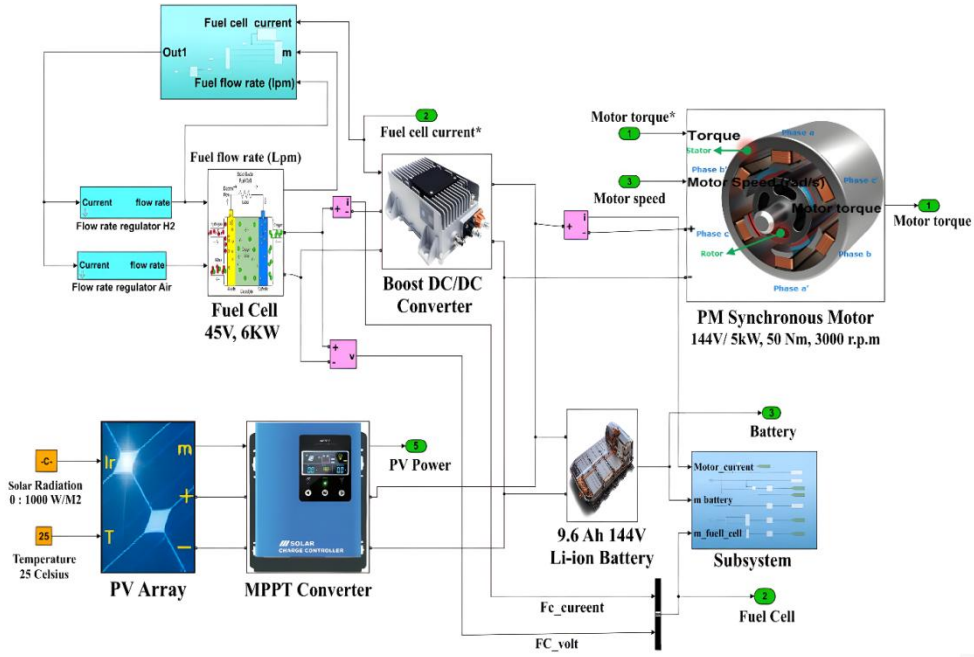

Figure 9. The electrical system of a photovoltaic-fuel cell-battery hybrid electric vehicle (PV-FC-battery HEV).

3.2.1 PV array and MPPT converter

The PV array model is constructed using an equivalent circuit embedded within a Simulink PV array block. The following equations present the mathematical models [28]. The solar cell current I is calculated as:

$$I = I_L - I_0 \left[\exp\left(\frac{q(V + IR_S)}{nkT} \right) - 1 \right] \quad (4)$$

Where V is the cell voltage, I_o is the diode saturation current, T is the cell temperature (Kelvin), q is the charge of an electron, n is the diode quality factor, and k is Boltzmann's constant. The current source I_L in Equation (4) is defined as:

$$I_L = I_{SC}\left(1 + \alpha_t(T - T_{ref})\frac{G}{G_{ref}}\right) \quad (5)$$

Where G_{ref} is the nominal solar irradiance, assumed to be 1000 W/m²; I_{SC} is the reference nominal short-circuit current under standard conditions; α_t is the temperature coefficient; and T_{ref} is the temperature for standard conditions, set at 25°C. The diode saturation current I_O is defined as:

$$I_0 = I_{0(ref)}\left[\left(\frac{T}{T_{ref}}\right)^3 \exp\left(\frac{-qE_g}{nk}\left(\frac{1}{T} - \frac{1}{T_{ref}}\right)\right)\right] \quad (6)$$

Where E_g is the bandgap voltage, and $I_{0(ref)}$ is the saturation current under standard conditions. The MPPT converter continuously adjusts the operating point of the PV panel to ensure it operates at the maximum power point for the given irradiation and temperature. The converter employs the Perturb and Observe (P&O) algorithm-based MPPT technique. The roof area of a typical lightweight vehicle is approximately 2 m², allowing for the installation of up to a 500 W PV array. The specifications of the PV array for the 6 kW class lightweight PVFCHEV studied here are detailed in Table 4.

Table 4. The specifications of the PV array.

Parameter	Value	Unit
Series-connected modules	2	Piece
Cells per module	72	Piece
Maximum current at MPP	5.84	A
Maximum voltage at MPP	42.8	V
Short circuit current (I_{sc})	6.2	A
Open circuit voltage (V_{oc})	50.93	V
Maximum power per module	250	W

Abbreviation: PV, photovoltaic.

3.2.2 Fuel Cell and Boost Converter

The model of the PEMFC stack is based on the detailed fuel cell stack model provided in Simulink. The mathematical representation of the PEMFC is presented in the following equations [29]. The voltage of the fuel cell stack V_{FC} is:

$$V_{FC} = E_{OC} - NA\ln\left(\frac{i_{FC}}{i_0}\right)\frac{1}{\frac{sT_d}{3} + 1} - Ri_{FC} \quad (7)$$

Where E_{OC} is the open circuit voltage, i_{FC} is the current of the FC stack, A is the Tafel slope, i_o is the exchange current, N is the number of cells, T_d is the reaction time, and R is the internal resistance. The open circuit voltage E_{OC} is:

$$E_{OC} = K_C E_n \tag{8}$$

Where K_C is the voltage constant under nominal operating conditions, and E_n is the Nernst voltage. The exchange current i_o is calculated as:

$$i_0 = \frac{zFk\left(P_{H_2} + P_{O_2}\right)}{Rh} e^{\frac{-\Delta G}{RT}} \tag{9}$$

Where z represents the number of moving electrons, F is Faraday's constant, k is Boltzmann's constant, R is the ideal gas constant, h is Planck's constant, T is the cell temperature in Kelvin (K), ΔG is the size of the activation barrier, P_{H2} is the partial pressure of hydrogen, and P_{O2} is the partial pressure of oxygen inside the stack in atmospheres (atm). The Tafel slope A is shown as:

$$A = \frac{RT}{z\alpha F} \tag{10}$$

Where α is the charge transfer coefficient. The partial pressure of hydrogen and oxygen is expressed as:

$$P_{H_2} = \left(1 - U_{fH_2}\right) x\,\% P_{fuel} \tag{11}$$

$$P_{fO_2} = \left(1 - U_{fO_2}\right) y\,\% P_{air} \tag{12}$$

Where P_{fuel} is the fuel pressure, U_{fH2} (%) is the nominal utilization rate of hydrogen, *x%* % is the percentage of hydrogen in the fuel, P_{air} is the air pressure, U_{fO2} (%) is the nominal utilization rate of oxygen, and *y%* % is the percentage of oxygen. The utilization rates of hydrogen and oxygen are calculated as follows:

$$U_{fH_2} = \frac{6000RTNi_{FC}}{zFP_{fuel}V_{fuel}x\%} \tag{13}$$

$$U_{fH_2} = \frac{6000RTNi_{FC}}{2zF\,P_{air}V_{air}\,y\%} \tag{14}$$

In this context, V_{fuel} (L/min) indicates the flow rate of hydrogen fuel, while V_{air} signifies the airflow rate.

The DC-DC converter for the fuel cell (FC) employs a boost-type configuration, and a proportional-integral (PI) controller manages the FC's power by tracking the reference current (i_{FC}) set by the ANN controller. Figure 10 depicts the control scheme of the converter, and Table 5 provides detailed specifications of the FC based on the parameters from the embedded Simulink model.

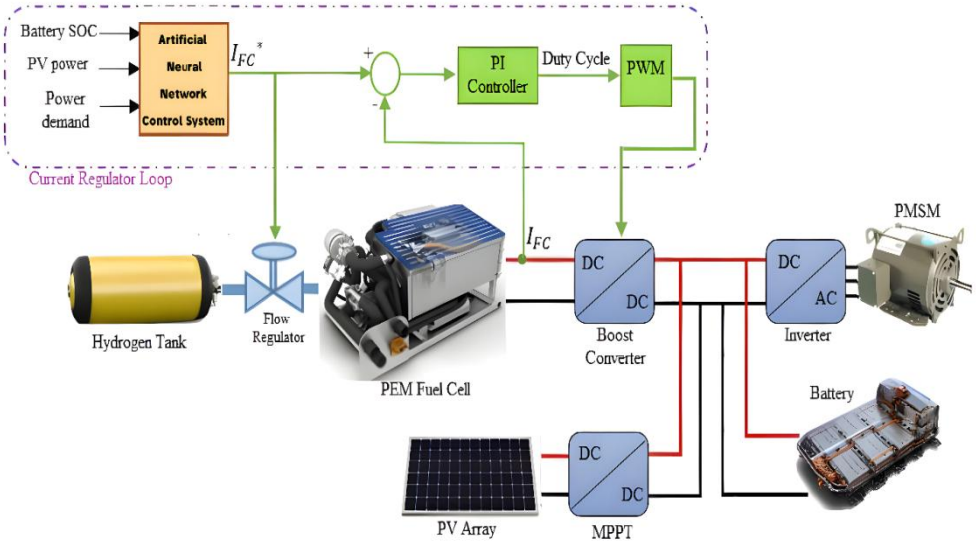

Figure 10. The control strategy for the fuel cell boost converter includes maximum power point tracking (MPPT), proton exchange membrane (PEM) technology, and the utilization of a permanent magnet synchronous machine (PMSM).

Table 5. The specifications of PEMFC.

Parameter	Value	Unit
Number of cells	65	Piece
Nominal voltage	45	V
Nominal power	4.2	KW
Peak power	6	KW
Fuel supply pressure	1.5	Bar
Operating temperature	65	°C
Nominal stack efficiency	55	%

3.2.3 Battery and Electric Motor

A Li-ion battery pack is utilized, with its dynamic model detailed in Reference [21]. For the lightweight electric vehicle (EV), the DC bus voltage is set at 144 V, which is lower than that of conventional EVs due to considerations of safety, cost, and technical performance. The battery pack is composed of 10 individual lithium-ion modules, each module comprising four NMC cells. Each cell has a nominal voltage of 3.6 V and a capacity of 9.6 Ah. As a result, the complete battery configuration yields a total voltage of

144 V and a total capacity of 9.6 Ah, suitable for the energy requirements of the proposed PVFCHEV system.

The electric motor is a 144 V, 5 kW interior permanent magnet synchronous motor (PMSM), paired with a driver based on the PM Synchronous Motor [22] Drive (AC6) block available in Simulink. This motor drive incorporates a closed-loop speed control system using the vector control method. In this research, the PMSM's maximum torque is specified as 50 Nm, and its maximum motor speed is 3000 rpm.

3.3 Vehicle dynamics

The vehicle dynamics system models the mechanical transmission components of the Vehicle, as shown in Figure 11. This model focuses exclusively on regenerative braking, emphasizing the performance of both the electrical system and the energy management system (EMS). For this analysis, road inclination and wind speed are set to zero. Vehicle specifications can be found in Table 6.

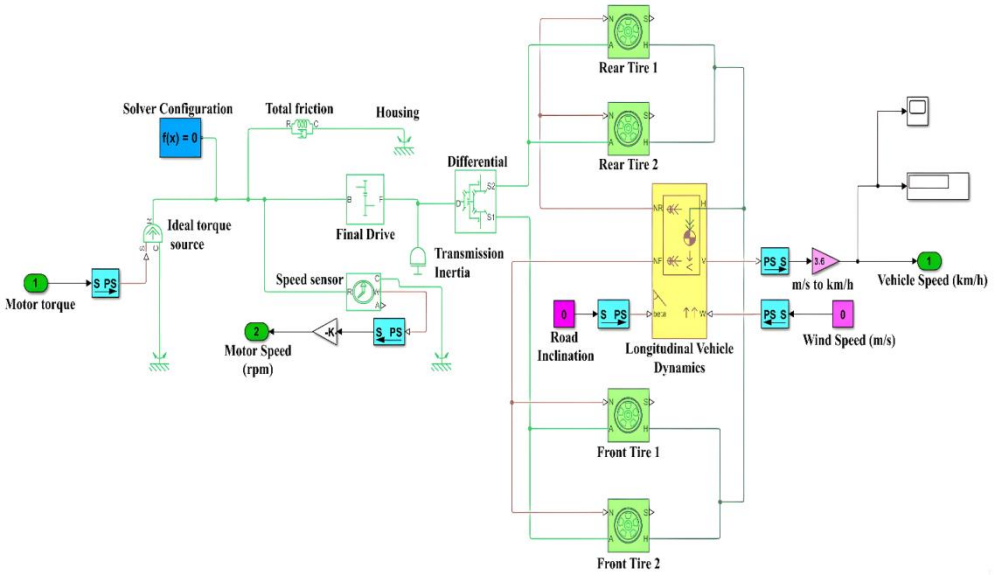

Figure 11. The block diagram of the vehicle dynamics system.

Table 6. The main parameters of the PVFCHEV.

Parameter	Value	Unit
Total mass	**800**	**Kg**
Maximum speed	**60**	**Km/h**
Frontal area	**2.3**	**M^2**
Rolling radius of the tires	**0.2**	**M**
Wheelbase	**2.5**	**M**
Gear ratio of the final drive	**3.0**	**-**
Aerodynamic drag coefficient	**0.36**	**-**

4 SIMULATION RESULTS AND DISCUSSIONS

4.1 Functional test results

The functional test simulates the operation of the PV-FC-battery HEV in different modes throughout a driving cycle, which includes idling, starting, cruising, accelerating, and regenerative braking. The testing procedure is outlined as follows:

1. t = 0 – 2 seconds: The vehicle is stopped, and the PV array charges the battery.
2. t = 2 – 6 seconds: The pedal position is set to 70% (starting).
3. t = 6 – 11 seconds: The pedal is released to 25% (cruising).
4. t = 11 – 16 seconds: The pedal is pushed to 85% (accelerating).
5. t = 16 seconds: The pedal position is set to -70% (regenerative braking).

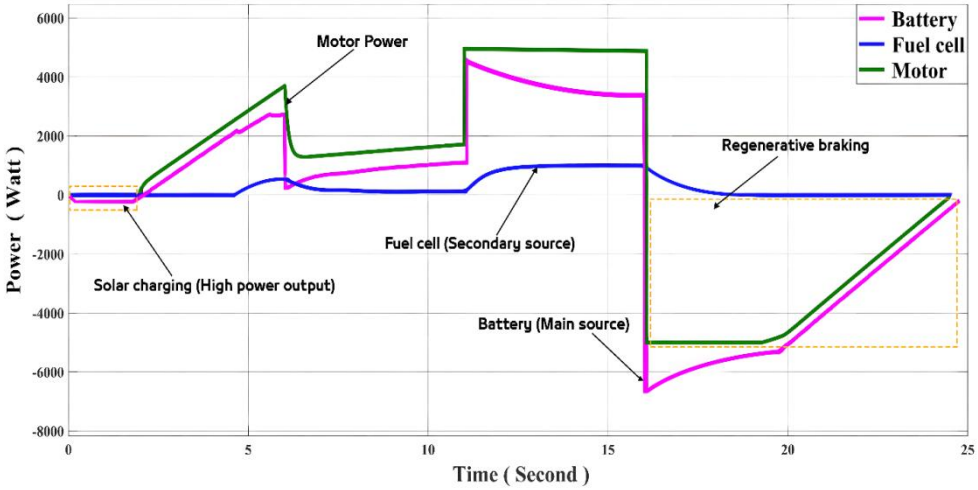

Figure 12. The power flow of the PVFCHEV system in the functional test.

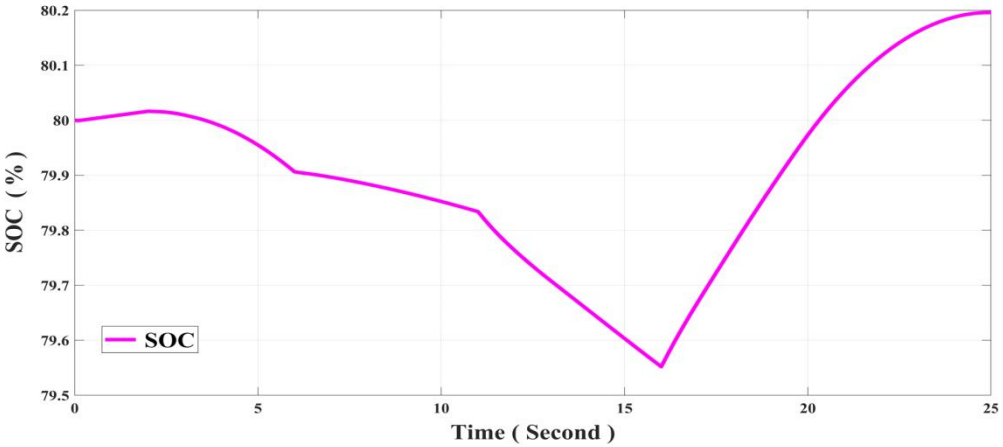

Figure 13. The battery state of charge (SOC) of the PVFCHEV system in the functional test.

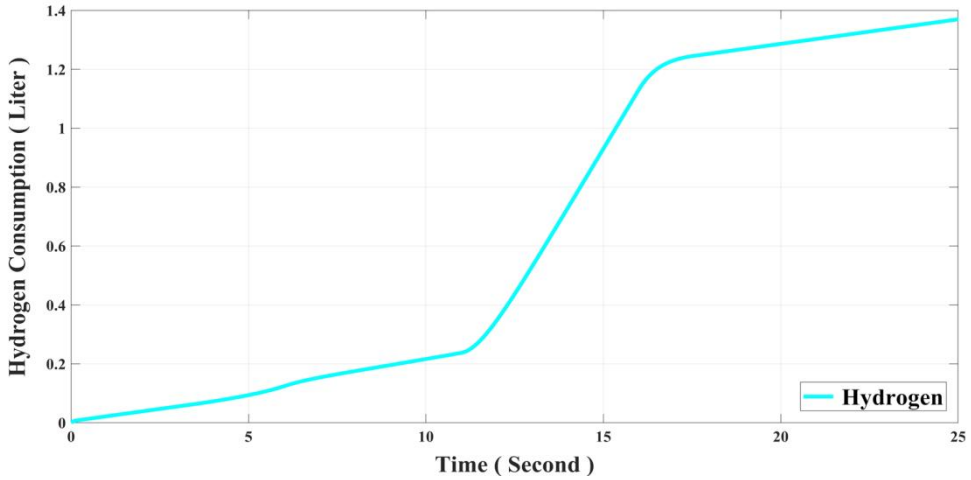

Figure 14. The hydrogen consumption of the PVFCHEV system in the functional test.

Figures 12, 13, and 14 illustrate the simulation results under conditions of 1000 W/m² solar radiance, a 25°C ambient temperature, and an initial battery state of charge (SOC) of 80%.

Given the intense solar radiation and high SOC of the battery, the battery acts as the primary power source. As shown in Figure 12, when the vehicle stops, the battery exhibits a negative power value, indicating that it is charging from solar energy.

During acceleration, both the battery and the photovoltaic (PV) array work together to power the vehicle until the fuel cell (FC) activates to meet the increased power demand. When the power demand decreases, the battery absorbs the excess power from the FC, which cannot immediately lower its output. At peak power, the battery remains the main power source, while the FC serves as a secondary source, helping to bring the battery's SOC to a more manageable level.

When the driver applies the brakes, the battery captures kinetic energy through regenerative braking, while the PV array continues to charge the battery. Figure 15 further illustrates the performance of the PVFCHEV under varying solar radiation levels and battery states.

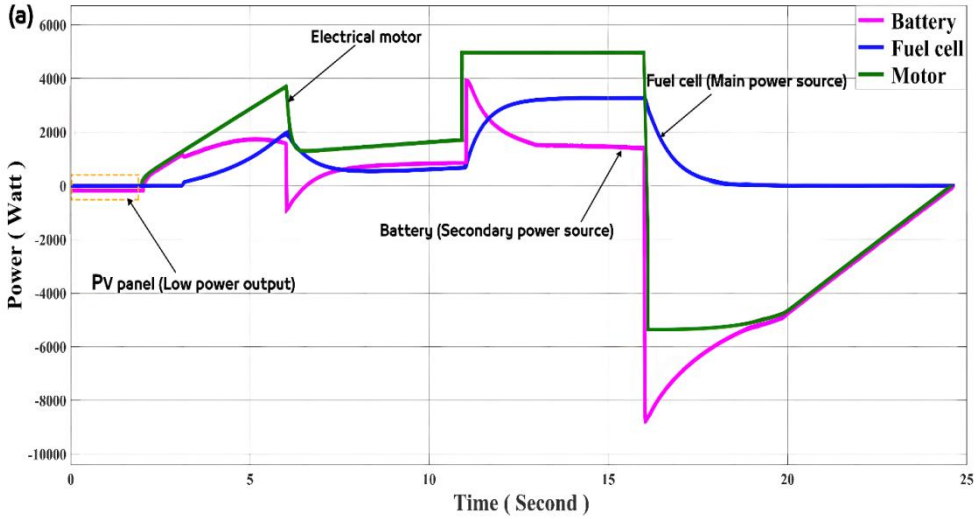

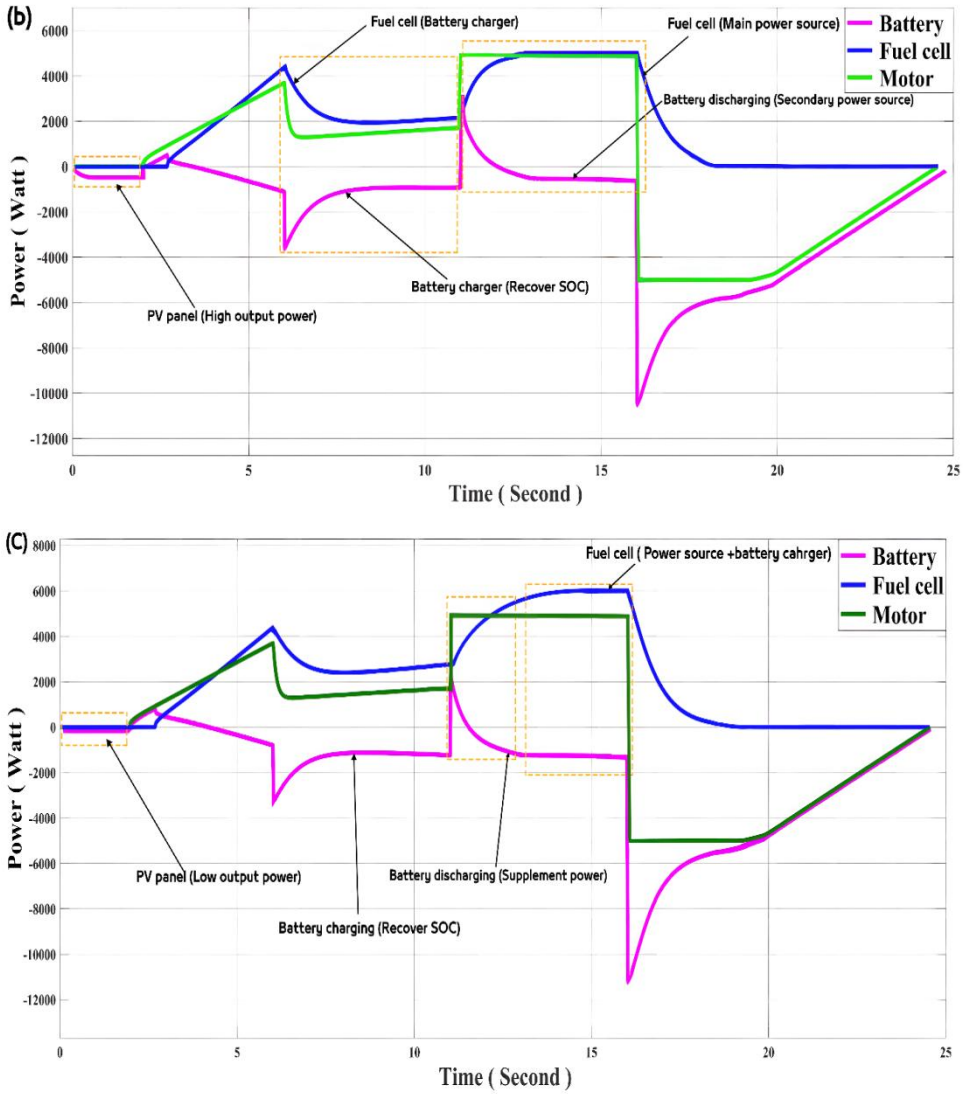

Figure 15. The performance of the PVFCHEV under different situations: A, Solar radiance = 400 W/m^2, initial battery SOC = 80%; B, Solar radiance = 1000 W/m^2, initial battery SOC = 30%; C, Solar radiance = 400 W/m^2, initial battery SOC = 30%. PVFCHEV, photovoltaic-fuel cell-battery hybrid electric vehicle; SOC, state-of-charge.

In Figure 15A, solar radiation is weak, and the battery's state of charge (SOC) is high. Consequently, the battery serves as a secondary power source, supplying a small fraction of the driving power.

In Figure 15B, abundant solar power coincides with a low battery SOC. In this scenario, the fuel cell (FC) becomes the primary power source, quickly charging the battery to restore its SOC. Given the strong solar radiation, it is essential to reserve some battery capacity for storing solar energy. As a result, when the motor requires peak power, the battery provides a small contribution, enabling the FC to operate with relatively high efficiency.

In Figure 15C, to prevent potential damage from over-discharging, the FC generates

additional power when both the battery SOC and solar power are low. The battery discharges only to compensate for any power deficit during vehicle acceleration.

Figures 12, 13, 14, and 15 illustrate that the electrical system of the photovoltaic fuel cell hybrid electric vehicle effectively carries out its key functions, including vehicle propulsion, power distribution regulation, and electric motor control. The energy management system (EMS) demonstrates strong performance even amid variations in solar radiation, battery status, and driving conditions.

4.2 Driving cycle test results

The World Harmonized Light-duty Test Procedures (WLTP) Class 1 driving cycle [30] is the standard used to assess the performance of lightweight (PVFCHEVs), as illustrated in Figure 16 and Table 7. This test simulates different environmental conditions and battery states.

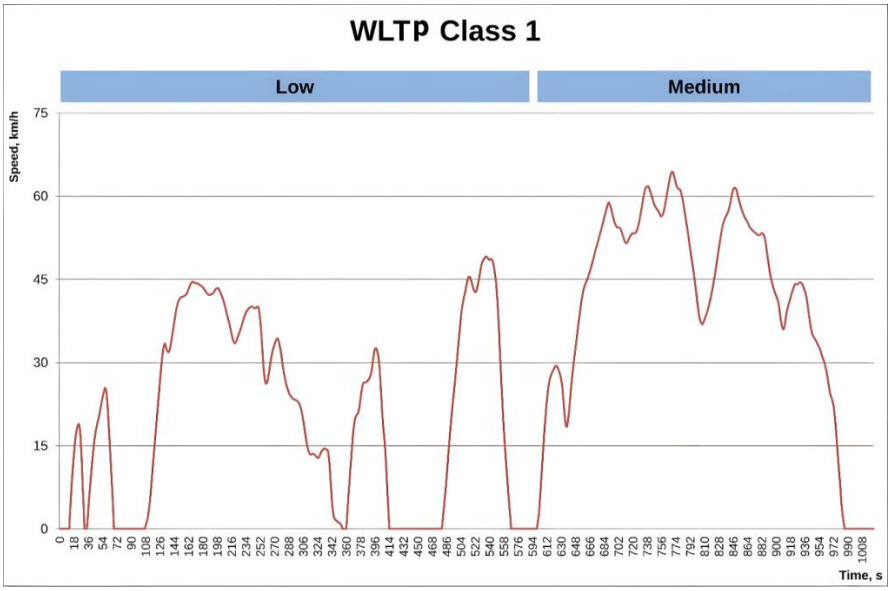

Figure 16. The World Harmonized Light-duty Test Procedures Class 1 driving cycle.

Table 7. The main parameters of the WLTP Class 1 driving cycle.

Parameter	Low	Medium	Total
Duration, S	589	433	1022
Stop duration, S	155	48	203
Distance, m	3324	4767	8091
% of stops	26.3 %	11.1 %	19.9 %
Maximum speed, Km/hr	49.1	64.4	
Average speed without stops, Km/hr	27.6	44.6	35.6
Average speed with stops, Km/hr	20.3	39.6	28.5
Minimum acceleration, m/s^2	-1	-0.6	
Maximum acceleration, m/s^2	0.8	0.6	

Abbreviation: WLTP, The World Harmonized Light-duty Test Procedures.

We have established three distinct scenarios that are detailed in the following sections.

Scenario 1: Under sunny conditions, with solar radiation measured at 1000 W/m², the photovoltaic (PV) array effectively charges the battery, increasing the initial state of charge is 80%.

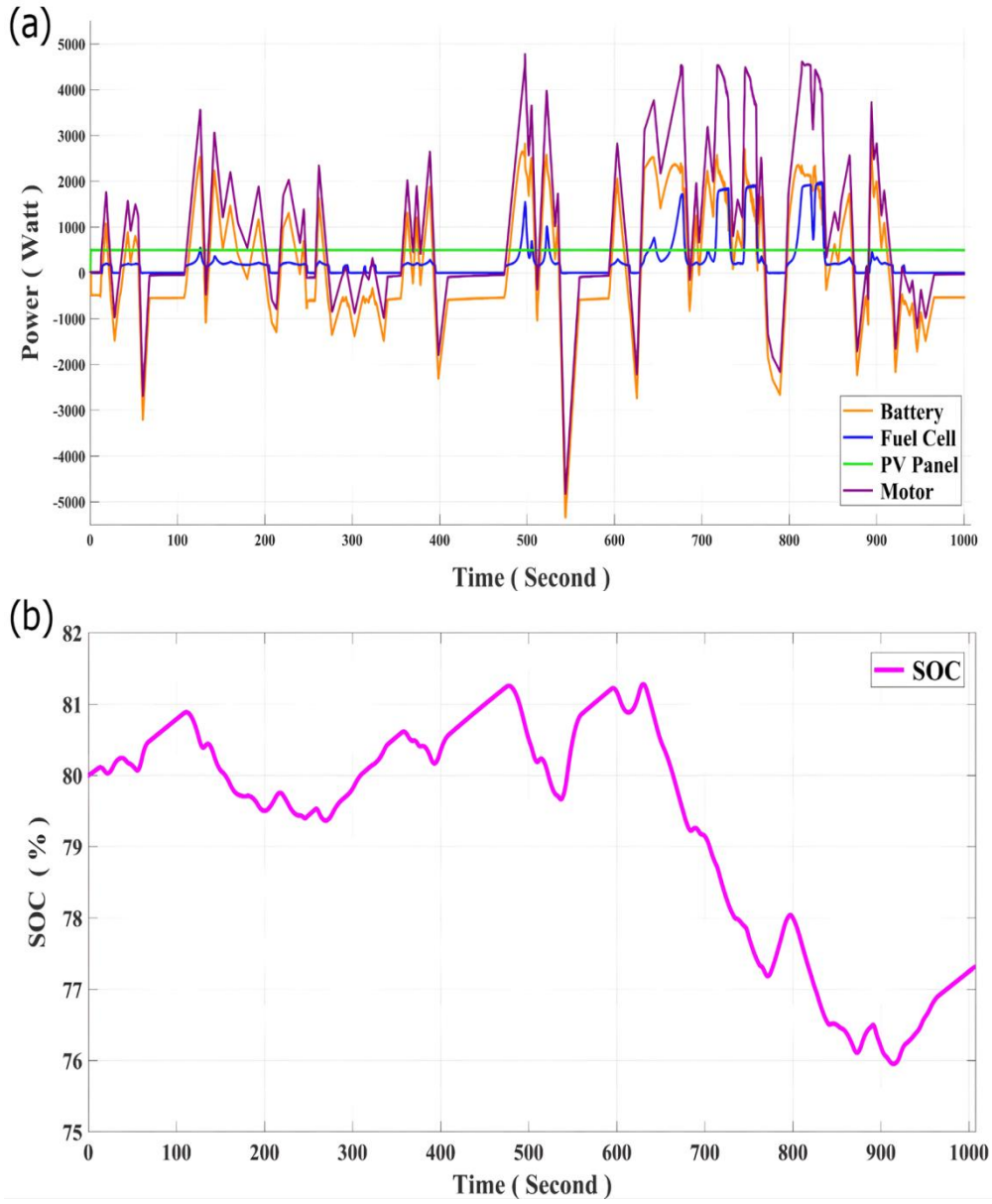

Figure 17. The performance of the PVFCHEV in Scenario 1: A, Power curves; B, Battery SOC curve. PVFCHEV, photovoltaic-fuel cell-battery hybrid electric vehicle; SOC, state-of-charge.

Figure 17 illustrates the power distribution of the photovoltaic-fuel cell hybrid electric vehicle (PV-FC-HEV) power system, along with the battery state of charge (SOC) for Scenario 1. In Figure 17A, the output power from the PV array is significant, enabling the battery to function as the primary power source as dictated by the energy management system (EMS). The fuel cell operates within a low power range, where its efficiency is relatively high, and remains inactive during periods of minimal power demand. The battery is designed to discharge its stored energy to optimize solar energy capture, resulting in a general decrease in the battery SOC, as depicted in Figure 17 B.

Scenario 2: In contrast, during overcast and rainy conditions, where solar radiation drops to 400 W/m², the power generated by the PV array is insufficient due to the reduced solar intensity, leading to an initial SOC of 30%.

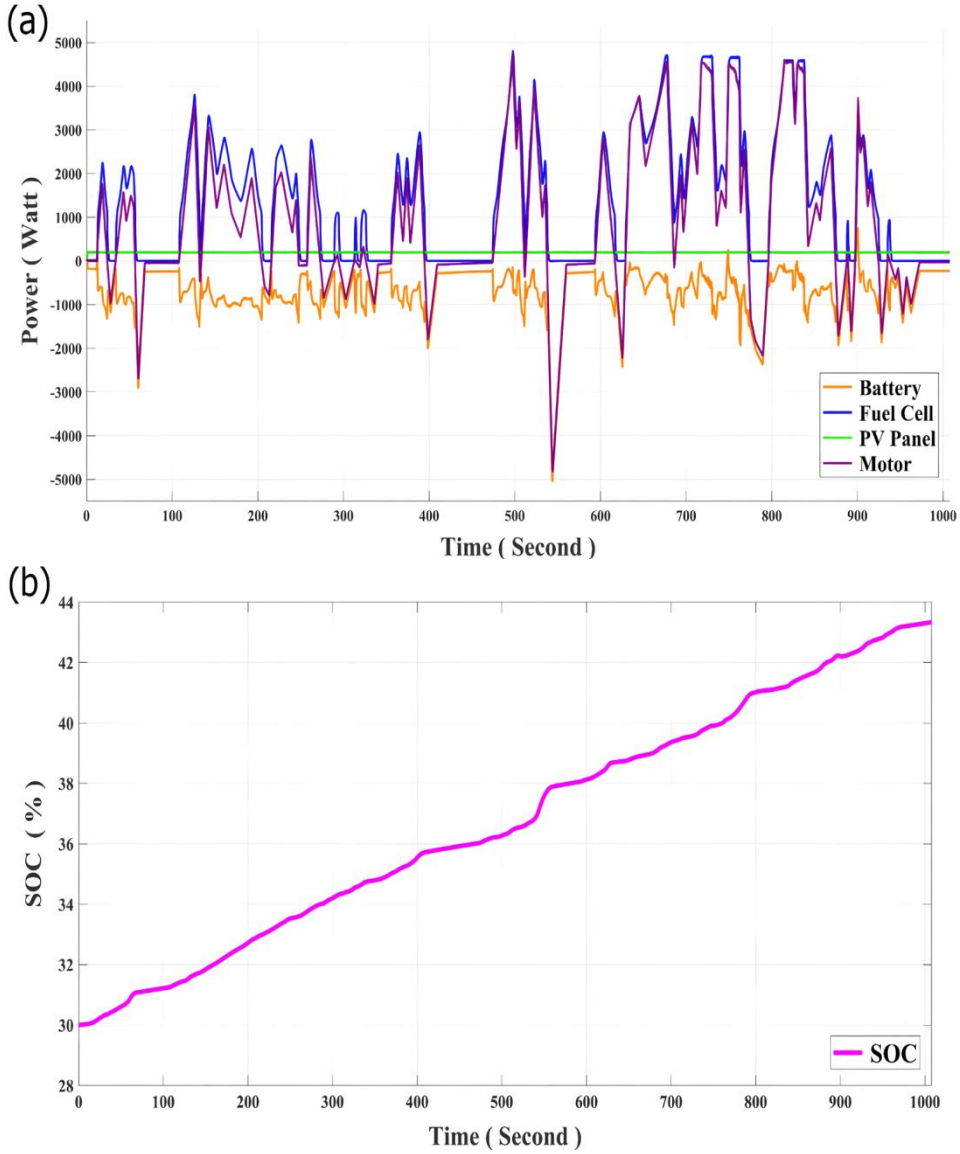

Figure 18. The performance of the PVFCHEV in Scenario 2: A, Power curves; B, Battery SOC curve. PVFCHEV, photovoltaic-fuel cell-battery hybrid electric vehicle; SOC, state-of-charge.

Figure 18 illustrates the power curves of the system and the battery state of charge (SOC) in Scenario 2. At the start, the fuel cell (FC) produces more power than is needed, intending to increase the battery SOC to a mid-level. When the battery SOC reaches around 40%, the FC decreases its excess power generation and starts to align with the power demand. This adjustment enables the battery to supply additional power for acceleration.

Scenario 3: At night, when solar radiation falls to 0 W/m², the PV array becomes inactive. Consequently, the power supplied to the vehicle comes solely from the fuel cell (FC) and the battery, which starts with an initial SOC of 50%.

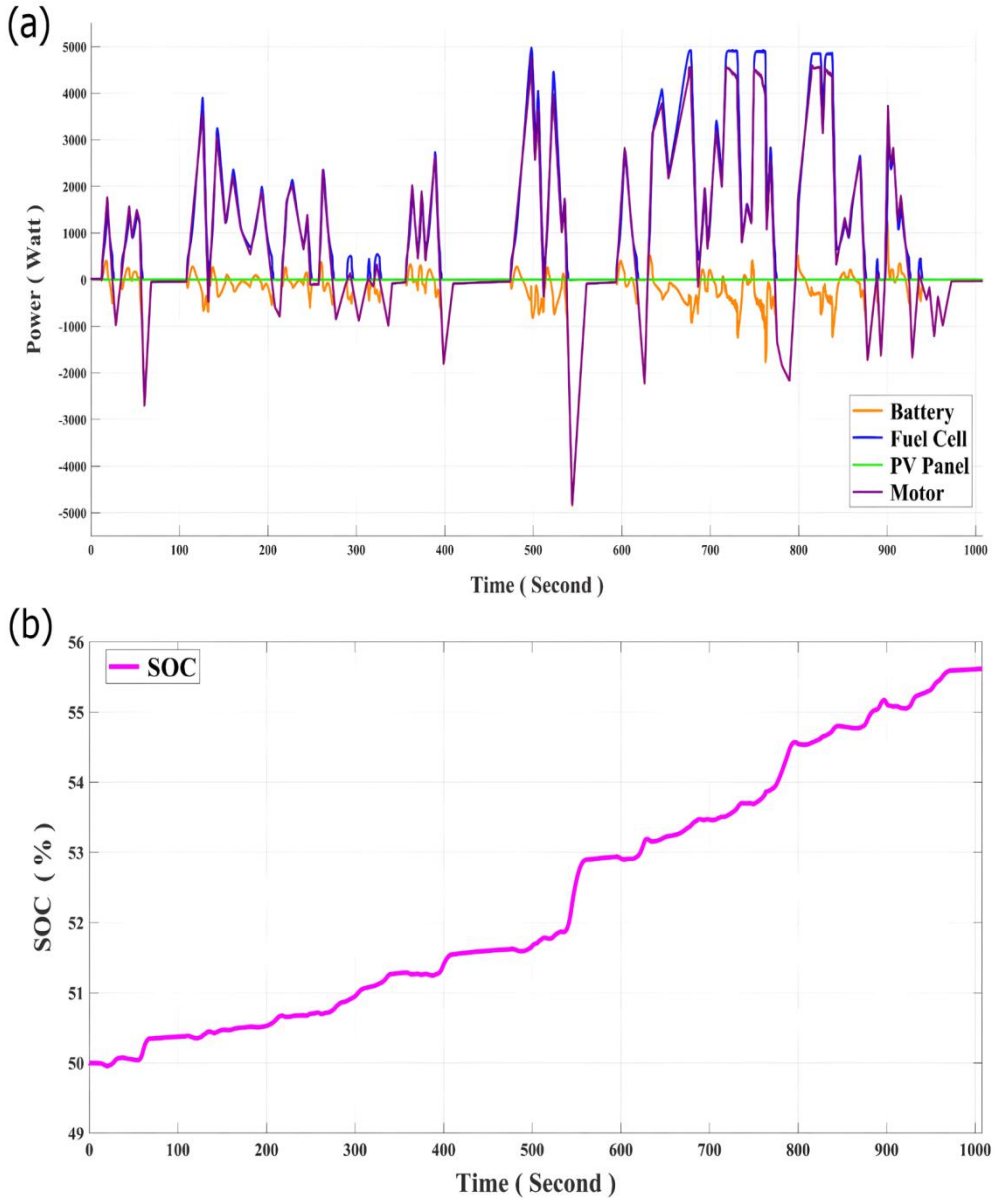

Figure 19. The performance of the PVFCHEV in Scenario 3: A, Power curves; B, Battery SOC curve. PVFCHEV, photovoltaic-fuel cell-battery hybrid electric vehicle; SOC, state-of-charge.

In the nighttime scenario, when the photovoltaic (PV) array is offline and only the fuel cells and battery are active, an Artificial Neural Network (ANN)-based power management strategy regulates the fuel cell output power in response to changes in thrust. In this setup, the fuel cell serves as the primary power source, while the battery acts as a temporary power source, as illustrated in Figure 19.

4.3 Comparison results between control systems

Scenario 1: Sunny. The solar radiation is 1000 W/m^2. The PV array charges the battery, and the initial battery SOC reaches 80% when starting.

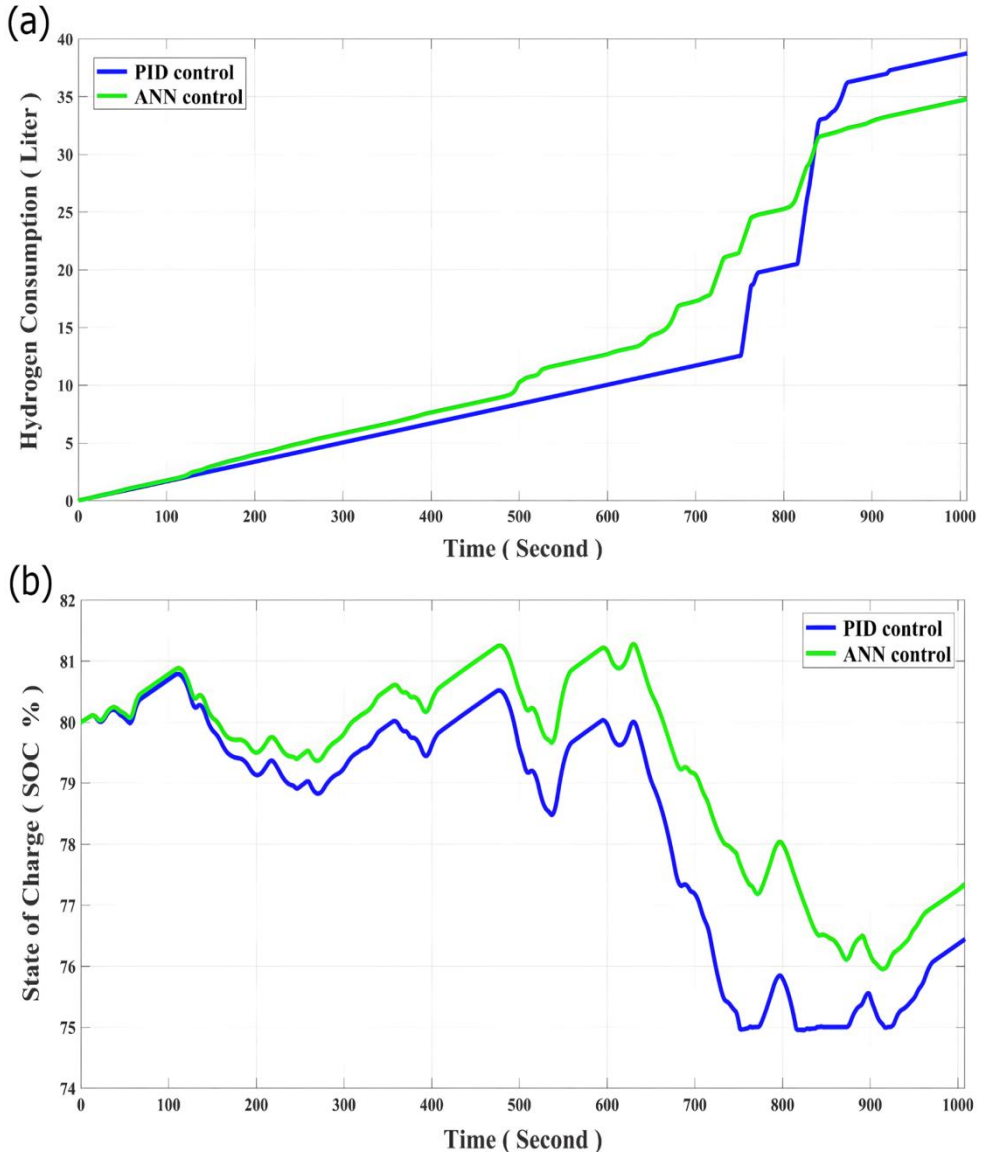

Figure 20. The comparison of different energy management strategies in Scenario 1: A, Hydrogen consumption; B, Battery SOC. SOC, state-of-charge.

Figure 20 illustrates the hydrogen consumption and battery state of charge (SOC) for the vehicle under two different energy management strategies. In Figure 20A, it is clear that the vehicle utilizing the PID strategy [31] consumes four liters more hydrogen than the one using the ANN strategy throughout the driving cycle. This increased hydrogen consumption is partially converted into electricity and stored in the battery, resulting in a higher SOC for the PID vehicle at the end of the test, as shown in Figure 20 B. However, this secondary energy transformation incurs energy losses, which can negatively impact overall energy efficiency and economic viability.

Scenario 2: Overcast/rainy. The solar radiation is 400 W/m^2. The PV power is insufficient in weak solar radiation, and the initial battery SOC is 30%

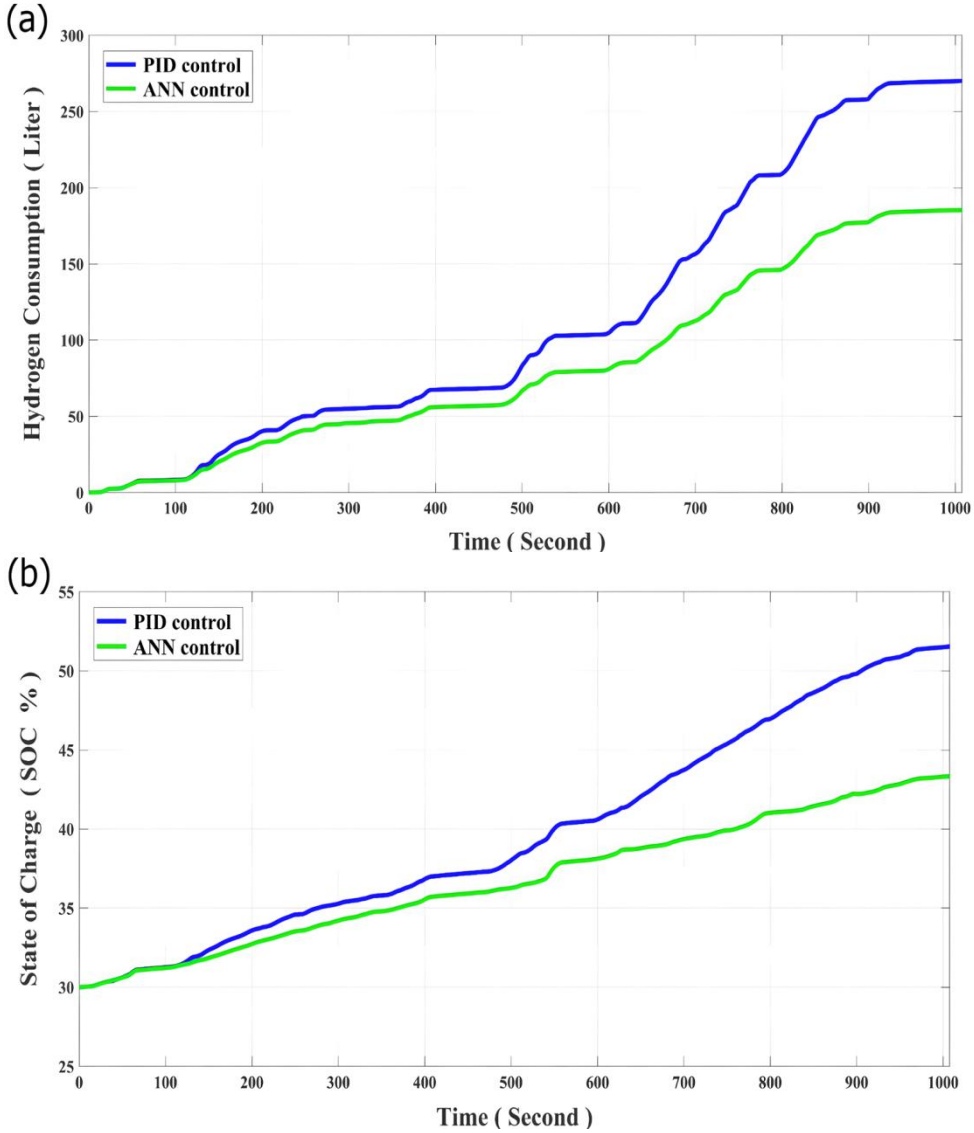

Figure 21. The comparison of different energy management strategies in Scenario 2: A, Hydrogen consumption; B, Battery SOC. SOC, state-of-charge

Figure 21 illustrates the hydrogen consumption and battery charge percentage for the vehicle employing two different energy management strategies. In Figure 21A, it is evident that under these operating conditions, the vehicle utilizing the PID strategy consumes eighty liters more hydrogen than the vehicle using the ANN strategy during the driving cycle, particularly in scenarios of low solar radiation and reduced battery charge percentage. This increased hydrogen consumption is partially converted into electricity and stored in the battery, leading to a higher battery charge percentage for the PID vehicle by the end of the test, as depicted in Figure 21 B. However, this secondary energy conversion incurs energy losses, which may diminish overall energy efficiency and economic feasibility.

Scenario 3: Night-time. The solar radiation is 0 W/m^2. The PV array does not work in this situation, and thus, only the FC and battery work to power the vehicle, and the initial battery SOC is 50%.

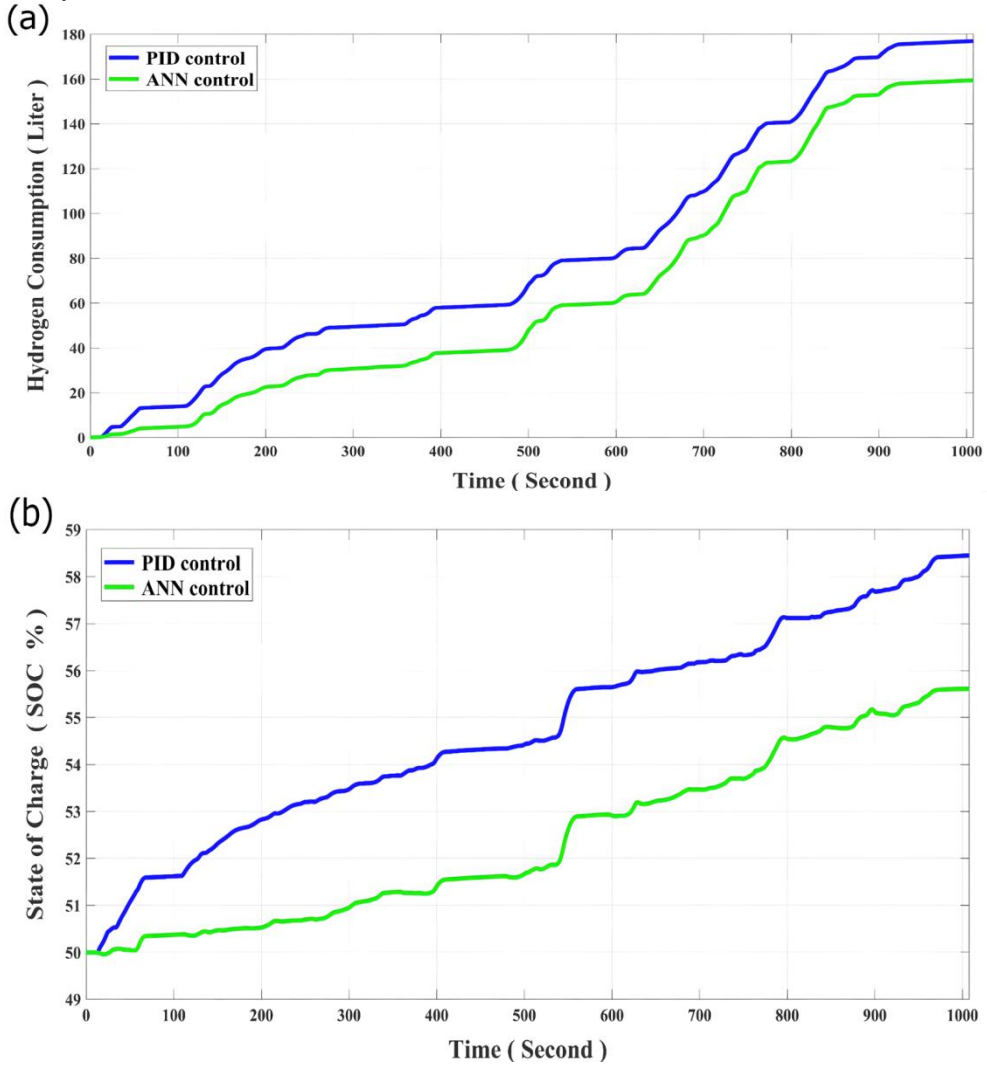

Figure 22. The comparison of different energy management strategies in Scenario 3: A, Hydrogen consumption; B, Battery SOC. SOC, state-of-charge.

Figure 22 illustrates hydrogen consumption and battery state of charge (SOC) for the vehicle under two energy management strategies during the night-time scenario when the photovoltaic array is offline and only the fuel cell (FC) and battery are in use. In Figure 22A, it is clear that the vehicle utilizing the PID strategy consumes seventeen liters more hydrogen than the vehicle using the ANN strategy throughout the driving cycle. This increased hydrogen consumption is partially converted into electricity and stored in the battery, resulting in a higher battery SOC for the PID vehicle at the end of the test, as depicted in Figure 22 B. However, this secondary energy conversion incurs energy losses, potentially reducing overall energy efficiency and economic viability.

The proposed EMS based on ANN offers significantly better fuel economy than the commonly used PID strategy. This improvement is due to the ANN enabling the fuel cell (FC) to operate within a high-efficiency range, whereas the PID simply adjusts the FC to match motor power. As a result, the PID approach consumes a larger amount of hydrogen and decreases the overall energy efficiency of the system.

5 CONCLUSIONS

This paper explores the technical feasibility of a hybrid electric vehicle (HEV) that combines photovoltaic (PV) systems, fuel cells (FC), and batteries (PV-FC-battery HEV). It employs a model-based approach to design an energy management strategy for the system. A lightweight PV-FC-HEV system with a capacity of 6 kW is modeled in the MATLAB/Simulink environment using a physics-based framework that includes the electrical system, energy management system (EMS), and vehicle dynamics. The EMS is developed using an artificial neural network (ANN) strategy that incorporates three input parameters: demand power, power output from the photovoltaic array, and the state of charge (SOC) of the battery. The output parameter is the reference power for the fuel cell. The goal is to efficiently manage power distribution among the various sources while maximizing the utilization of solar energy, considering its intermittent nature.

The model and Energy Management System (EMS) were validated through simulations of functional tests and driving cycle tests. The key findings are summarized as follows: during the functional tests, the designed electrical system effectively propels the vehicle and manages power distribution. These results further confirm the feasibility of a Photovoltaic Fuel Cell Hybrid Electric Vehicle (PVFCHEV) operating under varying levels of solar radiation and battery states. In the WLTP driving cycle test, the EMS successfully handles rapidly changing power demands, fluctuations in solar energy, and variations in the battery's state of charge (SOC). Furthermore, it demonstrates improved fuel economy when utilizing the Artificial Neural Networks control strategy, achieving savings of hydrogen fuel over the 8.1 km test compared to the Proportional-Integral-Derivative (PID) control strategy.

The modeling and simulations in this study lay the groundwork for future research, with a crucial emphasis on the need for experimental validation. Future efforts should focus on designing and executing experiments to validate the proposed PVFCHEV and its EMS. Fortunately, the physical model of the PVFCHEV developed here will assist in designing the experimental setup by integrating actual physical component models.

REFERENCES

[1] B. Zohuri, “Navigating the Global Energy Landscape Balancing Growth, Demand, and Sustainability,” pp. 1–7, Nov. 2023.

[2] M. A. Majid, C. R. K. J, and A. Ahmed, “Advances in electric vehicles for a self-reliant energy ecosystem and powering a sustainable future in India,” *e-Prime* -

Adv. Electr. Eng. Electron. Energy, vol. 10, p. 100753, 2024, doi: https://doi.org/10.1016/j.prime.2024.100753.

[3] M. Filonchyk, M. P. Peterson, L. Zhang, V. Hurynovich, and Y. He, "Greenhouse gases emissions and global climate change: Examining the influence of CO2, CH4, and N2O," *Sci. Total Environ.*, vol. 935, p. 173359, 2024, doi: https://doi.org/10.1016/j.scitotenv.2024.173359.

[4] I. Veza, M. Z. Asy'ari, M. Idris, V. Epin, I. M. Rizwanul Fattah, and M. Spraggon, "Electric vehicle (EV) and driving towards sustainability: Comparison between EV, HEV, PHEV, and ICE vehicles to achieve net zero emissions by 2050 from EV," *Alexandria Eng. J.*, vol. 82, pp. 459–467, 2023, doi: https://doi.org/10.1016/j.aej.2023.10.020.

[5] Q. Hassan, A. K. Al-Jiboory, A. Z. Sameen, M. Barakat, K. Y. M. Abdalrahman, and S. Algburi, "Transitioning to sustainable economic resilience through renewable energy and green hydrogen: The case of Iraq," *Unconv. Resour.*, vol. 5, p. 100124, 2025, doi: https://doi.org/10.1016/j.uncres.2024.100124.

[6] A. Gupta and A. K. Shukla, "Optimal approaches in global warming mitigation and adaptation strategies at city scale," *Discov. Sustain.*, vol. 5, no. 1, 2024, doi: 10.1007/s43621-024-00497-8.

[7] M. Khan Mk and N. Shahzad, "The Impact of Solar Charging Stations On the Power System," *Remit. Rev.*, vol. 9, pp. 1–14, Jul. 2024.

[8] F. M. I. Flora, "Assessment of concentrated solar power (CSP) generation potential in Cameroon using a Multi-Criteria Analysis Method and Geographic Information System (GIS)," *Heliyon*, vol. 11, no. 1, p. e41094, 2025, doi: https://doi.org/10.1016/j.heliyon.2024.e41094.

[9] A. Elnozahy, H. Abd-Elbary, and F. K. Abo-Elyousr, "Efficient energy harvesting from PV Panel with reinforced hydrophilic nano-materials for eco-buildings," *Energy Built Environ.*, vol. 5, no. 3, pp. 393–403, 2024, doi: https://doi.org/10.1016/j.enbenv.2022.12.001.

[10] M. Waseem, G. S. Lakshmi, M. Ahmad, and M. Suhaib, "Energy storage technology and its impact in electric vehicle: Current progress and future outlook," *Next Energy*, vol. 6, p. 100202, 2025, doi: https://doi.org/10.1016/j.nxener.2024.100202.

[11] C. Li, J. Na, K. Nan, J. Qin, and M. Wu, "Tesla's Product Improvement Strategies in the Electric Vehicle Market," *Adv. Econ. Manag. Polit. Sci.*, vol. 92, pp. 177–185, Jun. 2024, doi: 10.54254/2754-1169/92/20231197.

[12] M. Ali, K. Prakash, M. A. Hossain, and H. R. Pota, "Intelligent energy management: Evolving developments, current challenges, and research directions for a sustainable future," *J. Clean. Prod.*, vol. 314, p. 127904, 2021, doi: https://doi.org/10.1016/j.jclepro.2021.127904.

[13] J. J. Jui, M. A. Ahmad, M. M. I. Molla, and M. I. M. Rashid, "Optimal energy management strategies for hybrid electric vehicles: A recent survey of machine learning approaches," *J. Eng. Res.*, vol. 12, no. 3, pp. 454–467, 2024, doi: https://doi.org/10.1016/j.jer.2024.01.016.

[14] M. Rasool, M. A. Khan, and R. Zou, "A Comprehensive Analysis of Online and Offline Energy Management Approaches for Optimal Performance of Fuel Cell Hybrid Electric Vehicles," *Energies*, vol. 16, no. 8. 2023. doi: 10.3390/en16083325.

[15] A. Boukerche, Y. Tao, and P. Sun, "Artificial intelligence-based vehicular traffic flow prediction methods for supporting intelligent transportation systems," *Comput. Networks*, vol. 182, p. 107484, 2020, doi: https://doi.org/10.1016/j.comnet.2020.107484.

[16] K. Rajamani, C. Lefurgy, S. Ghiasi, J. Rubio, H. Hanson, and T. Keller, *Power management solutions for computer systems and data centers*. 2008. doi: 10.1145/1393921.1393956.

[17] S. G. Nnabuife, A. K. Hamzat, J. Whidborne, B. Kuang, and K. W. Jenkins, "Integration of renewable energy sources in tandem with electrolysis: A technology review for green hydrogen production," *Int. J. Hydrogen Energy*, 2024, doi: https://doi.org/10.1016/j.ijhydene.2024.06.342.

[18] L. Liberti, P. Milano, P. Zza, and L. Vinci, "Introduction to global optimization," Mar. 2006.

[19] Y. E. Altun and O. A. Kutlar, "Energy Management Systems' Modeling and Optimization in Hybrid Electric Vehicles," *Energies*, vol. 17, no. 7, 2024. doi: 10.3390/en17071696.

[20] J. Wu and Y. Zhao, "Machine learning technology in the application of genome analysis: A systematic review," *Gene*, vol. 705, pp. 149–156, 2019, doi: https://doi.org/10.1016/j.gene.2019.04.062.

[21] M. Khalid, "A Review on the Selected Applications of Battery-Supercapacitor Hybrid Energy Storage Systems for Microgrids," *Energies*, vol. 12, p. 4559, Nov. 2019, doi: 10.3390/en12234559.

[22] D. Mehta, R. Kumar, and P. Shah, *Application of Permanent Magnet Synchronous Motors in Electric Drive Systems*. 2024. doi: 10.1109/ICOCWC60930.2024.10470565.

[23] R. Paz, "The Design of the PID Controller," Jan. 2001.

[24] R. Zangmo *et al.*, "Optimal placement of renewable distributed generators and electric vehicles using multi-population evolution whale optimization algorithm," *Sci. Rep.*, vol. 14, no. 1, pp. 1–19, 2024, doi: 10.1038/s41598-024-80076-z.

[25] N. Bizon, "Load-following mode control of a standalone renewable/fuel cell hybrid power source," *Energy Convers. Manag.*, vol. 77, pp. 763–772, 2014, doi: https://doi.org/10.1016/j.enconman.2013.10.035.

[26] A. Peer Mohamed, K. R. M. Vijaya Chandrakala, S. Balamurugan, U. Subramaniam, and D. Almakhles, "Adaptive maximum power extraction technique in fuel-cell integrated with novel DC-DC converter topology for low-power electric vehicle applications," *Eng. Sci. Technol. and Int. J.*, vol. 54, p. 101723, 2024, doi: https://doi.org/10.1016/j.jestch.2024.101723.

[27] A. Agwa and M. Alruwaili, "MPPT of PEM Fuel Cell Using DC-DC Boost Converter Based on SVM," *PRZEGLĄD ELEKTROTECHNICZNY*, vol. 100, pp. 53–58, Oct. 2024, doi: 10.15199/48.2024.11.10.

[28] F. Ghani, G. Rosengarten, M. Duke, and J. K. Carson, "The numerical calculation of single-diode solar-cell modeling parameters," *Renew. Energy*, vol. 72, pp. 105–112, 2014, doi: https://doi.org/10.1016/j.renene.2014.06.035.

[29] M. Sharma, R. Pachauri, and S. Goel, *MATLAB/Simulink modeling and analysis of parametric effects on PEMFC performance*. 2015. doi: 10.1109/RDCAPE.2015.7281400.

[30] M. Tutuianu *et al.*, "Development of the Worldwide harmonized Light duty Test Cycle (WLTC) and a possible pathway for its introduction in the European legislation," *Transp. Res. Part D Transp. Environ.*, vol. 40, pp. 61–75, 2015, doi: https://doi.org/10.1016/j.trd.2015.07.011.

[31] G. Çetin, O. Özkaraca, and A. Keçebaş, "Development of PID-based control strategy in maximum exergy efficiency of a geothermal power plant," *Renew. Sustain. Energy Rev.*, vol. 137, p. 110623, 2021, doi: https://doi.org/10.1016/j.rser.2020.110623.